Unique Crack Propagation of Double Network Hydrogels under High Stretch

Ye Zhang[a], Kazuki Fukao[a], Takahiro Matsuda[b], Tasuku Nakajima[b,c,d], Katsuhiko Tsunoda[e], Takayuki Kurokawa[b], and Jian Ping Gong[b,c]*
[a]Graduate School of Life Science, Hokkaido University, Sapporo 001-0021, Japan
[b]Faculty of Advanced Life Science, Hokkaido University, Sapporo 001-0021, Japan
[c]Institute for Chemical Reaction Design and Discovery, Hokkaido University, Sapporo 001-0021, Japan
[d]Japan Science and Technology Agency, PRESTO
[e]Advanced Materials Division, Bridgestone Corporation, Tokyo 187-8531, Japan
*Corresponding author. Email: gong@sci.hokudai.ac.jp

Abstract
Double network (DN) gels, consisting of two contrasting interpenetrated polymer networks, exhibit large resistances to crack initiation and propagation. For practical applications, crack resistances of materials in highly stretched states are important. In this study, we investigated the crack growth behaviors of DN gels in stretched states by inducing crack seeds into these gels under various degrees of tension. This examination enables the analysis of crack propagation for a wide range of bulk energy release rate G. The power-law relationship between G and crack growth velocity v was investigated for DN gels with different tensile behaviors. We found that for brittle and unnecking DN gels, the velocities changed from slow mode (quasi-stationary fracture) to fast mode (dynamic fracture) with an increase in G, similar to that of a single network gel; in contrast, for necking DN gels having higher crack resistances than those of the unnecking DN gels, only fast modes were observed once the G is above a threshold. Real-time birefringence observation reveals a large damage zone around the crack tip at G slightly lower than the threshold, while the damage zone is hardly observed at G higher than the threshold. The results indicate that, for the necking DN gels, crack initiation has a large energy barrier owing to the formation of the damage zone; once this barrier is overcome, the excess energy release accelerates the crack propagation and therefore the gels exhibit dynamic fracture.

Keywords:
Double network hydrogels
Crack propagation under tension
Energy release rate
Crack resistance
Dynamic fracture
Velocity jump

1. Introduction

The double network (DN) concept informs an effective approach for the fabrication of polymeric materials with outstanding mechanical strength and toughness [1–3]. A typical tough DN material comprises two interpenetrating polymer networks with contrasting mechanical properties. That is, one network is rigid and brittle, whereas the other network is soft and stretchable [1,2]. DN materials show significantly higher resistances to crack initiation and propagation than those of their individual components [2,4,5]. Synergistic effect of DN concept is related to the substantial internal fracture of the brittle network [6–10]. The rigid and brittle network bears the load; nevertheless, it breaks at relatively small deformations, and the load is transferred to the soft and stretchable network, which also deforms. Then, strain-hardening of the load-bearing soft network induces further fracture of the neighboring brittle network entangled with the soft network, thereby continuously expanding the "damage zone" [11]. This load transfer appears as a yielding-like phenomenon and a necking phenomenon during uniaxial tensile elongation [12,13]. During this process, a large amount of sacrificial fracture of covalent bonds can be generated in the brittle network, which results in large energy dissipation and considerably enhances the crack resistances of DN materials.

The DN effect was initially observed in hydrogels. Subsequently, the DN concept was applied to various types of polymeric materials such as hydrogels [3,14–17], elastomers [8,18,19], and composite materials [20–22], which considerably expanded the possible application ranges of soft materials. Specifically, in addition to high strength, toughness [23,24], and fatigue resistance [25], typical DN gels show high water retentions, low sliding frictions [26] and biocompatibilities [27] and have attracted significant attention as novel load-bearing biomaterials including artificial cartilages.

For various potential applications of DN materials, a clarification of fracture behaviors at various deformation states is indispensable. Previous studies on the fractures of DN hydrogels have mainly focused on the investigation of crack propagation from a pre-notched crack under monotonic loading by tearing tests [4,5,23,24,28–30]. On the other hand, the resistance to post-notched cracks in highly tensioned states has been hardly investigated for the DN gels. This property is also very important because such cracks can be accidentally inserted onto the loaded state during the usage like punctures of automotive tires by sharp nails. Because an unnotched sample can be loaded to a substantially higher tension than that of a pre-notched sample, the examination of post-notched crack propagation behaviors on unnotched samples enables the observation of fracture behaviors under overstretched state at which the crack could be accelerated by releasing of excess amount of elastic energy. Previously, using strip samples in pure shear geometries, the crack propagation dynamics at various input stretching energy has been investigated for soft materials such as rubbers, and an abrupt crack velocity jump from slow mode to fast mode is observed at increased stretching [31–33]. Kolvin *et al.* revealed that a typical DN gel showed unique crack tip shapes with fast crack propagation in a

highly stretched state [34]. From the perspective of application, fast-mode crack propagation may cause catastrophic failure of materials and thereby results in serious accident to customers.

The purpose of this study is elucidating the correlation between the double network structure and the crack growth behaviors at highly stretched state. We adopted DN hydrogels comprising the densely crosslinked polyelectrolyte poly(2-acrylamido-2-methylpropanesulfonic acid) (PAMPS) as the rigid and brittle network (first network) and the loosely crosslinked neutral polymer poly(acrylamide) (PAAm) as the soft and stretchable network (second network). We prepared DN gels with various network structures, which tuned their tensile behaviors from brittle to ductile. We analyzed the mode I crack growth behaviors of DN gels in stretched states by inducing crack seeds into these gels under various degrees of tension. We determined the power-law relationship between the strain energy release rate of the bulk sample G and the crack growth velocity v at steady state. We performed real-time birefringence observation to characterize the damage zone of the samples around the crack tips. Finally, we analyzed the relationship between uniaxial tensile behaviors and crack growth behaviors and discussed the effect of the damage zone on the crack propagation behavior under tension.

2. Materials and Methods

2.1 Materials

2-Acrylamido-2-methylpropanesulfonic acid (AMPS; Toa Gosei, Co., Ltd.) was used as received. Acrylamide (AAm; Junsei Chemical, Co., Ltd.) was recrystallized from acetone. *N*,*N*′-Methylenebisacrylamide (MBAA; FUJIFILM Wako Pure Chemical Corporation) and 2-oxoglutaric acid (*α*-keto; FUJIFILM Wako Pure Chemical Corporation) were used as received.

2.2 Gel Synthesis

PAMPS/PAAm DN gels with the same first network compositions but different second network compositions were prepared (Table 1). DN gels consisting of PAMPS as the first network and PAAm as the second network were synthesized by the same procedures as previously reported [23]. The precursor PAMPS aqueous solution, containing 1 M AMPS as a monomer, 3 mol% MBAA as a crosslinker, and 1 mol% *α*-keto as an initiator (both relative to the monomer concentration), was poured into a glass mold consisting of two pieces of glass plates separated by a 0.5 mm silicone rubber spacer. Then, the glass mold was irradiated with ultraviolet (UV) light for 6 h under an argon atmosphere for the synthesis of PAMPS gels by free-radical polymerization. The synthesized PAMPS gels were immersed in four different precursor PAAm aqueous solutions, containing AAm at different concentrations (0.8, 1.2, 1.6, and 2.0 M), 0.01 mol% MBAA, and 0.01 mol% *α*-keto (both relative to the monomer concentration), for at least 1 day until the PAMPS gels reached swelling equilibrium. Due to the osmotic pressure of the counter ions, the

PAMPS gels considerably swelled, and the precursor PAAm aqueous solutions were incorporated into the PAMPS gels. Subsequently, the swollen PAMPS gels were sandwiched between two glass plates and irradiated with UV light for 8 h under an argon atmosphere for the synthesis of PAAm. A DN gel with a high crosslinker concentration of PAAm was also prepared from the precursor aqueous solution comprising 2.0 M AAm, 0.1 mol% MBAA, 0.01 mol% α-keto (both relative to the monomer concentration). The obtained DN gels were soaked in pure water for at least 3 days to remove unreacted reagents and to reach a new swelling equilibrium. The as-prepared DN gels only slightly swelled in pure water because PAMPS had already highly swelled in the precursor PAAm aqueous solutions, and the swelling of PAAm was suppressed by PAMPS. The thicknesses of the samples were slightly different because of different swelling ratios at equilibrium; however, the thicknesses of all the samples were in the range of 1.0–1.4 mm. The pre-stretch ratio of PAMPS in the swollen DN sample with respect to that of its as-prepared state, λ_s, is presented in Table 1. λ_s was estimated from the thickness of the swollen DN gel and the PAMPS gel during preparation (0.5 mm).

As reference samples, PAAm SN gels were also fabricated from an aqueous solution containing 2.0 M AAm, 0.01 mol% MBAA, and 0.01 mol% α-keto using a 1 mm thick silicone spacer. The PAAm gels were used in the as-prepared state without being swollen in water to maintain the SN concentration similar to that of the second network in the DN gel that hardly swelled after preparation.

For simplicity, DN gels were denoted as DN-C_2(-x_2), where C_2 (M) and x_2 (mol%) are the monomer concentration and the crosslinker concentration of the precursor PAAm aqueous solution. Unless otherwise stated, x_2 was 0.01 mol%. Similarly, the SN gels were represented as SN-C_2.

Table 1. A list of formulations and properties of the samples used in this study.

Sample code	Composition of the second network			λ_s [m/m]	Tensile behavior	$\lambda_s\lambda_y$ [m/m]	$\lambda_s^2\sigma_y$ [MPa]
	AAm C_2 [M]	MBAA x_2 [mol%]	α-keto [mol%]				
SN-C_2	2.0	0.01	0.01	−	Stretchable	−	−
DN-C_2(-x_2)	0.8	0.01	0.01	2.54 ± 0.04	Brittle	−	−
	1.2			2.45 ± 0.03	Necking	9.13 ± 0.15	3.79 ± 0.08
	1.6			2.50 ± 0.06	Necking	8.59 ± 0.21	3.60 ± 0.18
	2.0			2.69 ± 0.10	Necking	9.04 ± 0.33	3.93 ± 0.28
	2.0	0.1		2.39 ± 0.07	Unnecking	−	−

All the concentrations mentioned are the in-feed concentrations used in the precursor solutions. For DN gels, the first network formulations were the same, whereas the second network formulations were different. λ_s is the pre-stretch ratio of the first network in the DN gel. Tensile behaviors were characterized by the uniaxial stress–strain curves shown

in Fig. 2. $\lambda_s\lambda_y$ and $\lambda_s^2\sigma_y$ are the stretch ratio and the nominal stress at yielding point normalized by λ_s, as shown in Fig. S1.

2.3 Uniaxial Tensile Test

Uniaxial tensile tests were conducted on samples cut into dumbbell shapes (gauge length: 12 mm and width: 2 mm) using a commercial tensile tester (Instron 5965, Instron Co.). The tensile velocity was fixed at 50 mm/min, corresponding to an initial strain rate of 0.07 s^{-1}. Young's moduli E of the gels were estimated from the initial slopes of the nominal stress (σ)–tensile strain (ε) curves in the strain range of 0.05–0.15.

2.4 Crack Growth Test with Real-Time Birefringence Image Observation

Dynamic fracture tests of the samples in pure shear geometries were performed using the procedure schematically shown in Fig. 1a. At first, the samples were clamped in rectangular shapes with 50 mm width and 10 mm initial height (l_0). Then, the samples were stretched to a preset strain at a tensile velocity of 50 mm/min (Tensilon RTC-1150A, Orientec Co.). Thereafter, a ~10 mm long cut was created at one edge of the sample in the center using sharp scissors, and the crack propagation behaviors were observed by a polarized high-speed camera (CRYSTA PI-1P, Photron Co., Ltd.) [35]. The camera captured images at a rate of 3000 frames per second for short-term measurements or 60 frames per second for long-term measurements. From the acquired images, images showing crack propagation were extracted, and the time profiles of the crack length were obtained using ImageJ. For crack propagation in high-speed near shear wave speed, Goldman *et al*. demonstrated using a PAAm gel that crack acceleration becomes significantly sluggish at time $t \sim l_0/c_s$, owing to the interaction with the reflected elastic waves from the sample's vertical boundaries ("acquisition of inertia"), which results in the steady-state of v [36]. The cracks of our samples at fast speed also actually become approximately steady state within $l_0/c_s \sim 10^{-3}$–10^{-2} s as shown in Fig. S2 (l_0 = 10 mm and $c_s \sim$ 1–10 m/s). Therefore, v was estimated from the region where the crack propagated at a constant speed (Fig. S2). Simultaneously, to investigate molecular orientation around the cracks of DN gels, retardation R in each pixel of the images was also evaluated. Owing to the limitation of the measurement system, the discernible range of R was within 130 nm, corresponding to one-fourth of the light source wavelength (520 nm). The resolutions of the gray-scale images were approximately 80 μm/pixel, whereas those of the polarized light images were 160 μm/pixel. To avoid drying of samples in air, we set the maximum measurement times within ~100 seconds. Therefore, the minimum detection limit of v was ~10^{-6} m/s in this study.

The energy release rate of the sample at preset strain $G(\varepsilon)$ was calculated from the σ–ε curves of unnotched samples with the same pure shear geometries as the notched samples by the following equation:

$$G(\varepsilon) = W_{el}(\varepsilon) \times l_0 \qquad (1)$$

where $W_{el}(\varepsilon)$ is the stored elastic strain energy density of the sample stretched to the strain ε and l_0 is the initial sample height [37,38]. For a purely elastic material, $W_{el}(\varepsilon)$ is determined from the area under the loading σ–ε curve. However, DN gels showed large mechanical hysteresis (Mullins effect) during the loading–unloading process, as schematically depicted in Fig. 1b, because a certain amount of input energy was irreversibly dissipated by the fracture of PAMPS during sample stretching. The PAAm gel also demonstrated weak mechanical hysteresis due to the physical interaction between polymer chains (Fig. S3). Therefore, the area under the unloading σ–ε curve $W_{unloading}(\varepsilon)$ can be taken as $W_{el}(\varepsilon)$ to calculate the G in this study. To obtain $G(\varepsilon)$, we conducted cyclic tensile tests of the samples in pure shear geometries using a commercial tensile tester (Shimadzu Autograph AG-X universal tensile machine, Shimadzu Co.) at a tensile velocity of 50 mm/min. At first, the samples were loaded to a small strain of $\Delta\varepsilon$ and unloaded to the initial point. Then, the samples were loaded to $2\Delta\varepsilon$ and unloaded to the initial point. This process was repeated for n steps (n = 1, 2, ...) until the samples reached the yielding points or fractured (Fig. S3). The area under the unloading curve of the step n under the maximum strain $\varepsilon_{max,n} = n\Delta\varepsilon$ was evaluated as follows:

$$W_{unloading,n}(\varepsilon_{max,n}) = -\int_{\varepsilon_{max,n}}^{0} \sigma_{unloading}(\varepsilon)d\varepsilon \qquad (2).$$

The relationship between $\varepsilon_{max,n}$ and $W_{unloading,n}(\varepsilon_{max,n})$ for various samples is shown in Figs. S4a and S4b. The $W_{unloading,n}$–$\varepsilon_{max,n}$ relations of SN-2.0 and brittle DN-0.8 were fitted by quadratic regression, whereas those of the other DN samples were fitted by linear regression. G as a function of the applied strain was estimated from the regression curves of $W_{unloading,n}(\varepsilon_{max,n})$ using equation (1).

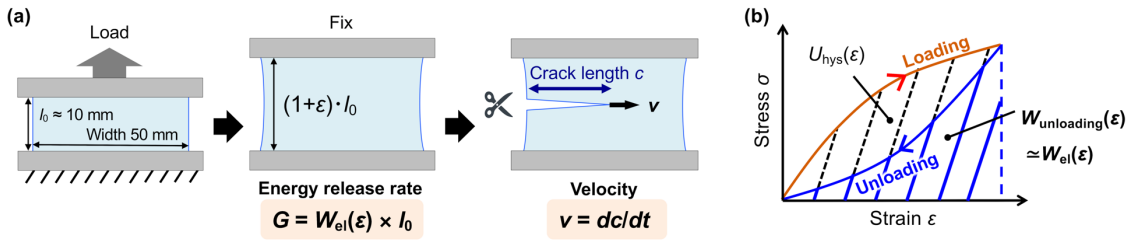

Fig. 1. (a) Schematics of crack growth test. Left: pure shear geometry of the test sample, middle: sample at stretching prior to notching, and right: crack propagation after notching. (b) Stress–strain curves of the energy stored in typical DN gels. The red curve represents the loading stress–strain curve, and the blue curve depicts the unloading stress–strain curve. The black hatched area indicates the dissipated energy, U_{hys}, and the blue hatched area represents the stored strain energy of the fixed sample, W_{el}.

3. Results and Discussion

3.1 Uniaxial Tensile Behavior

Figure 2 depicts the σ–ε curves of the SN and DN gels with different formulations measured by uniaxial tensile tests. Because the SN gel corresponding to the second network was loosely crosslinked, it was very stretchable; nevertheless, it broke at a relatively small stress. All the DN gels showed almost the same E because the first network compositions were nearly the same in these DN gels (Table 2). The DN gel with a low second network concentration (DN-0.8) easily fractured at a low fracture strain and low fracture stress, and this DN gel is defined as "brittle" DN gel hereinafter. In contrast, all the DN gels with high C_2 values (1.2–2.0 M) demonstrated yielding behaviors along with necking around the strain ε_y ~2.2, at which the stress quickly decreased initially and then plateaued. Thus, these samples are defined as "necking" DN gels hereinafter. The fracture strains of these necking DN gels increased with an increase in C_2; DN-1.2 fractured in the plateau region with a relatively low strain, whereas DN-1.6 and DN-2.0 showed distinct strain hardenings with large fracture strains.

As suggested in previous works, below the yielding point, internal fracture of the first network diffusively occurs, whereas above the yielding point, a large internal crack formed in the first network, and the second network strands, that may bridge the crack between the broken first network clusters, carry the load and are highly stretched [7,10]. Notably, the slightly different yielding points for the three necking DN gels are owing to the slightly different swellings of their first networks. After normalization by the pre-stretch ratio of the first network λ_s (Table 1 and Fig. S1), the σ–ε curves and yielding points almost overlapped. These results confirmed that below the yielding point, the mechanical behaviors of the DN gels are governed by the first network, irrespective of C_2 for the necking DN gels [13,24].

For the DN gel with a tightly crosslinked second network (DN-2.0-0.1), no abrupt decrease in stress and no plateau region were noticed, as indicated by the orange line in Fig. 2. The sample did not exhibit necking and a clear yielding point. Hereinafter, we denote this DN gel as "unnecking" DN gel.

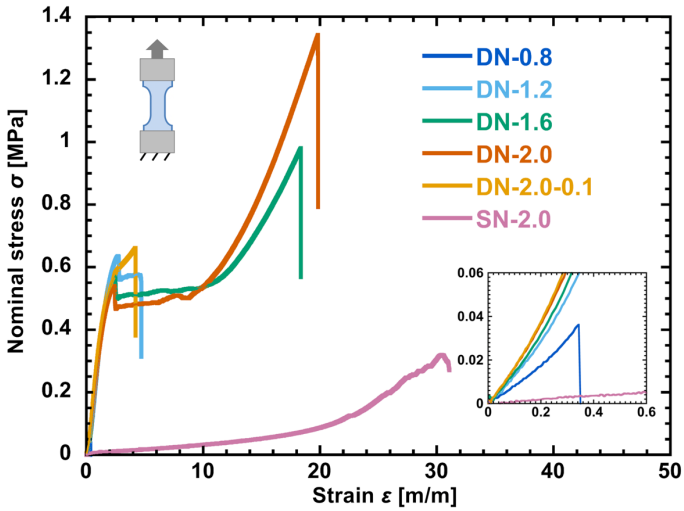

Fig. 2. Uniaxial tensile stress–strain curves of SN-2.0 and the DN gels with different concentrations of the second network and crosslinking densities. The inset shows the magnified stress–strain curves of brittle DN-0.8. The inset image depicts a schematic of the uniaxial tensile test. The sample codes are provided in Table 1.

3.2 Crack Growth Behaviors Under Tension

Figure 3 shows the optical images of the crack growth behavior, and Fig. 4 depicts the power-law relationship between G and v for each sample. For SN-2.0, when the sample was cut at relatively low G, the crack propagated at very slow speeds (for example, v = 2.4 × 10^{-4} m/s at G = 3.38 × 10^{2} J/m^2, Fig. 3a and Movie S1). When the sample was cut at a relatively high G, the crack propagated at a very high speed (for example, v = 2.7 × 10^{0} m/s at G = 9.35 × 10^{2} J/m^2). From the G–v logarithmic plots of SN-2.0, the velocity jump was observed at a certain G (Fig. 4a). This phenomenon is similar to those noticed in the cases of filled elastomers [31,39], and we denote this critical value of energy release rate for velocity jump as G_{jump} in this study. For SN-2.0, the G_{jump} was approximately 4.5 × 10^{2} J/m^2, below which the crack propagated at very slow speeds (v = 10^{-4}–10^{-3} m/s), whereas, above which the cracks propagated at very high speeds (v = 10^{0}–10^{1} m/s).

Brittle DN-0.8 also demonstrated the velocity jump phenomenon but at a much lower G_{jump} (≈ 6.0 × 10^{1} J/m^2) than that of SN-2.0, below which the crack propagated at very slow speeds (v = 10^{-3}–10^{-2} m/s), whereas above G_{jump}, the crack propagated at very high speeds (v > 10^{0} m/s; Fig. 3b and Movie S2). As DN-0.8 was too brittle to load to large G reproducibly, its fast-mode crack propagations only could be measured in low frame rate; nevertheless, we confirmed that v was at least more than 1.1 × 10^{0} m/s at G = 6.29 × 10^{1} J/m^2.

Unexpectedly, the necking DN gels showed unique crack propagation behaviors. As shown in Fig. 3c, the cracks in these samples did not propagate even at relatively large G values. However, the cracks started to propagate at very fast speeds (v = 10^{0}–10^{1} m/s; Movie S3) once G reached a threshold (denoted as G_{th}, hereinafter) of approximately 1.6

$\times 10^3$ J/m^2, and slow speed crack propagation was not observed (Figs. 4a and 4b). We verified that the necking DN gels could suppress crack propagation even with a large notch (approximately 10 mm) under high tension. For example, in the case of DN-2.0, the crack did not propagate at $\varepsilon \leq 2.3$, $\sigma \leq 0.52$ MPa, and $G \leq 1.55 \times 10^3$ J/m^2. We verified that the crack propagation could not be observed below G_{th} at least for 100 seconds, when the effect of sample drying in air was assumed to be negligible. As shown in Table 2, G_{th} of the necking DN gels slightly increased with an increase in C_2. In contrast, unnecking DN-2.0-0.1 with almost the same C_2 but a higher crosslinking density demonstrated a slow-mode crack propagation ($v = 10^{-5}$–10^{-3} m/s; Fig. 3d and Movie. S4), and the slow-mode crack propagation switched to the fast-mode crack propagation at $G_{jump} \approx 1.35 \times 10^3$ J/m^2 (Fig. 4a). G_{jump} of the unnecking DN-2.0-0.1 is slightly lower than G_{th} of the corresponding necking DN-2.0.

Because the maximum crack propagation speed is limited by the shear wave speed (c_s) of materials, we normalized the v by $c_s = \sqrt{\mu/\rho}$, where μ is the shear modulus of the virgin samples and ρ is the mass density of the gels (Table 2). As shown in Fig. 4c, all v in the fast-mode region converge when normalized by their corresponding c_s, and v/c_s lies in the 0.1–1 range, which means that v in the fast mode approaches its maximum value.

In the slow-mode region where v is considerably lower than the shear wave velocity, the crack growth is in a quasi-stationary state with negligible inertia effect, and G is balanced by the rate-dependent fracture energy $\Gamma(v)$, namely, $\Gamma(v) = G$. According to the positive G dependence of v as shown in Fig. 4a, $\Gamma(v)$ slightly increases with v in the slow-mode region.

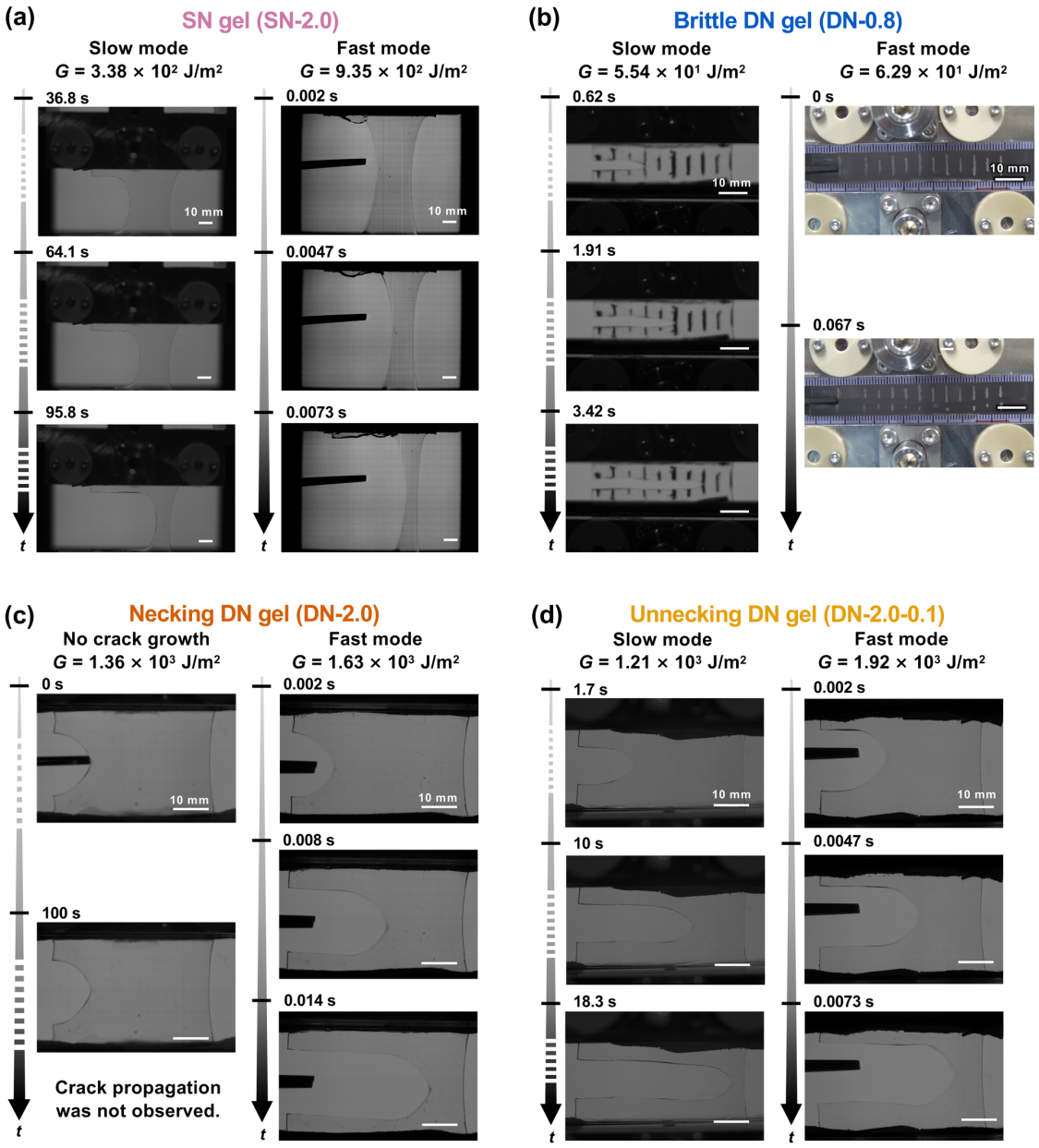

Fig. 3. Representative optical images showing the crack growth behaviors of (a) SN-2.0, (b) DN-0.8, (c) DN-2.0, and (d) DN-2.0-0.1. Scale bars represent 10 mm.

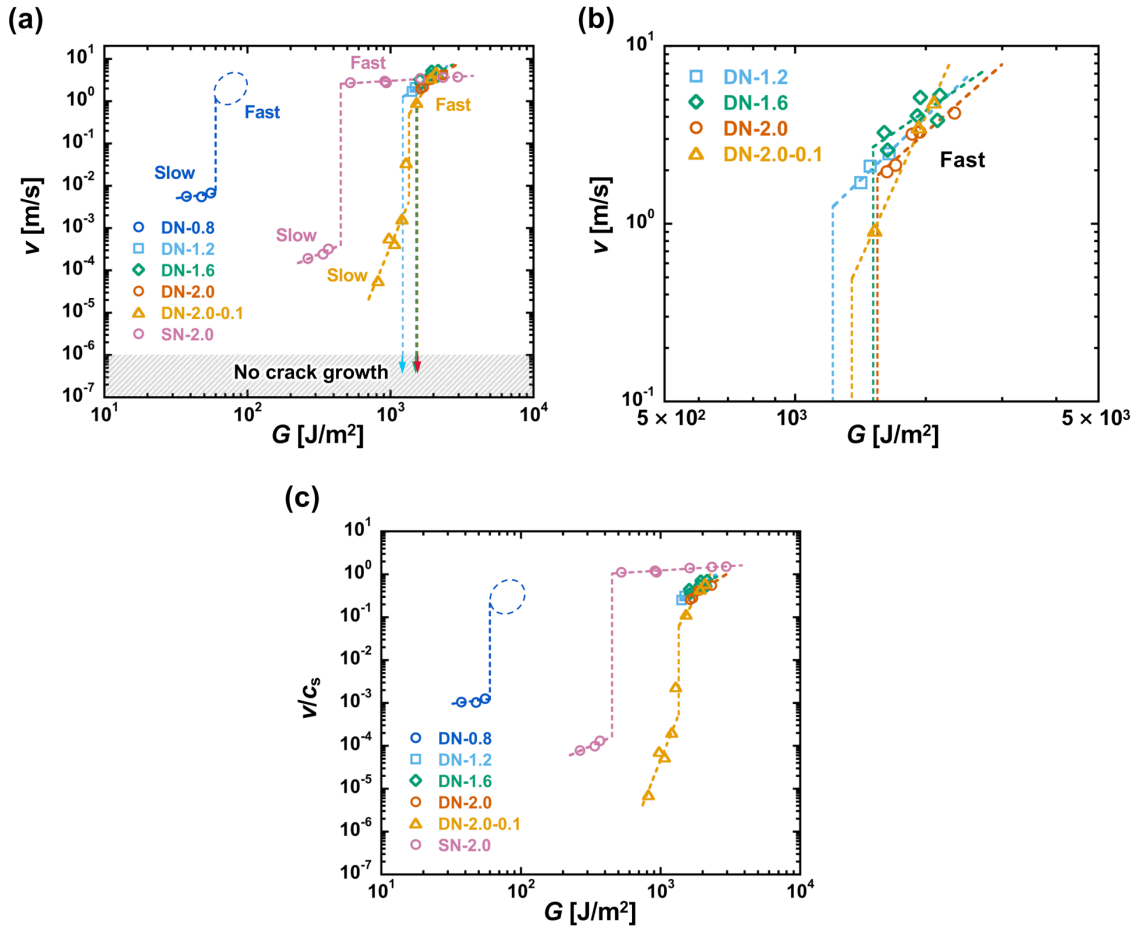

Fig. 4. (a) Logarithmic plots of the energy release rate G and the velocity of crack growth v measured by post-notch crack growth tests. The arrows depict the G at which crack propagation was not detected. The grey hatched regime indicates the crack propagation was not observed within experimental resolution (10^{-6} m/s). (b) Magnified images of the plots shown in (a) for the necking DN gels and unnecking DN-2.0-0.1 in the fast mode. (c) Logarithmic plots of G and v normalized by the shear wave speed c_s. The blue dashed circles in (a) and (c) represent the uncertainty of the crack velocity of DN-0.8 in the fast mode ($v > 1.1 \times 10^0$ m/s at $G = 6.29 \times 10^1$ J/m^2).

Table 2. A list of parameters related to crack propagation in the fast mode for the samples shown in Table 1.

Sample code	E [MPa]	c_s [m/s]	G_{jump} [J/m^2]	G_{th} [J/m^2]
SN-2.0	0.018 ± 0.006	2.4	≈ 4.5 × 10^2	–
DN-0.8	0.085 ± 0.004	5.3	≈ 6.0 × 10^1	–
DN-1.2	0.136 ± 0.013	6.7	–	≈ 1.3 × 10^3
DN-1.6	0.158 ± 0.007	7.3	–	≈ 1.55 × 10^3
DN-2.0	0.174 ± 0.005	7.6	–	≈ 1.6 × 10^3
DN-2.0-0.1	0.187 ± 0.008	7.9	≈ 1.35 × 10^3	–

E is the Young's modulus. c_s is the shear wave speed. $c_s = \sqrt{\mu/\rho}$ is calculated from the mass densities $\rho \approx 1$ g/cm^3 and the E by using the Poisson's ratio $\nu = 0.5$ and the shear modulus $\mu = E/2(1 + \nu) = E/3$ owing to the incompressibility of gels. For DN gels, E values of the virgin samples were used. G_{jump} is the critical value for the velocity jump from slow mode to fast mode of SN, brittle and unnecking DN gels, and G_{th} is the threshold value for the crack propagation of necking DN gels.

As G_{th} is the bulk energy release rate calculated from $G_{th} = W_{el}(\varepsilon_{th})l_0$, where ε_{th} is the critical strain for crack propagation at a certain initial sample height l_0, if G_{th} is the intrinsic critical G related to the crack propagation, it should not change with l_0. To confirm this, crack growth tests were performed on DN-2.0 with different l_0 (5, 8, and 15 mm) at a fixed sample width (50 mm). As shown in Fig. 5, the ε-v plots strongly depended on l_0 and the ε_{th} decreased with an increase in l_0, whereas the G-v plots almost collapsed on a master curve and the G_{th} hardly changed with an increase in l_0. This result verified that G_{th} is an intrinsic parameter, whereas ε_{th} is not. G_{th} is balanced with Γ_c, the energy dissipation for crack initiation, namely, $G_{th} = \Gamma_c$. It should be noted that the samples with smaller l_0 have larger ε_{th} and therefore larger amount of brittle network in the DN samples has already broken during the loading process, as revealed by the large mechanical hysteresis of the loading-unloading curves in Figs. S3 and S4. However, we noticed that G_{th} and the G-v plots are hardly affected by l_0, which indicates that the breakage of the sacrificial network in the loading process does not have a substantial impact on the crack initiation and propagation.

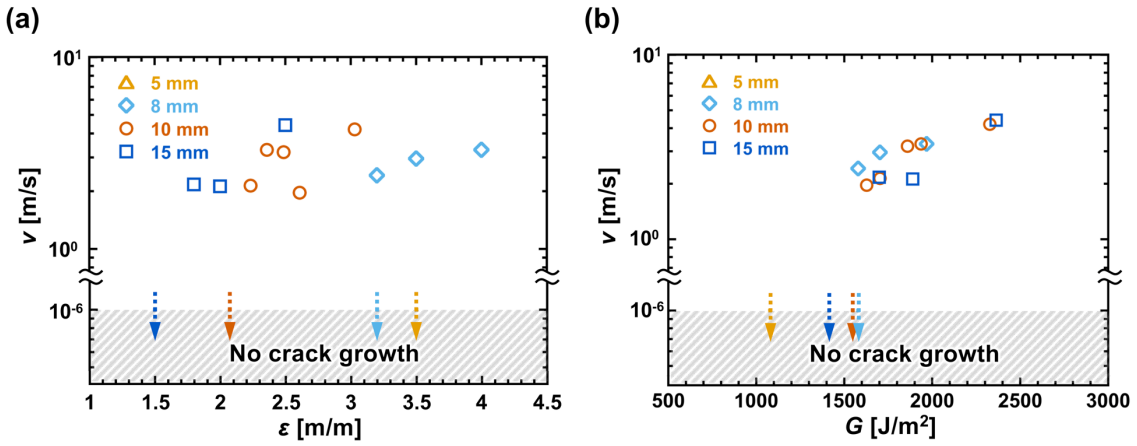

Fig. 5. The effect of initial sample height l_0 on the crack propagation of the necking DN gel (DN-2.0). (a) Crack velocity as a function of strain ε and (b) crack velocity as a function of the energy release rate G. The arrows depict the G at which crack propagation was not detected. The grey hatched regime indicates the crack propagation was not observed within experimental resolution. For the samples with smaller l_0 (= 5 and 8 mm), G at high ε (> 3) were calculated by the extrapolation of its $W_{\text{unloading},n}$–$\varepsilon_{\text{max},n}$ relation as shown in Fig. S5.

The above results indicate that for the necking DN gel, crack propagated above a large threshold energy release rate in fast mode. To determine whether the necking with yielding in the uniaxial tensile test and suppression of the slow-mode crack propagation were intrinsically correlated for DN gels with various structures, we further studied the behaviors of three DN gels with different first network composition (Table 3). Fig. 6 shows the tensile properties and crack propagation behaviors of the three DN gels. For comparison, the results of other previously discussed DN gels are also presented. All samples can be classified into two groups: DN gels showing necking and yielding behaviors in the σ–ε curves and DN gels only exhibiting certain strain softening but no necking (Fig. 6a). Again, as shown in Fig. 6b, all the necking samples did not demonstrate slow-mode crack propagation, whereas all the unnecking samples showed slow-mode crack propagation. Although no significant differences were noticed between the tensile fracture stresses of DN-1.2 and DN-2.0-0.1, and between DN-N2 and DN-U1, depending on whether necking and yielding occurred or not, considerable differences were observed between the crack propagation behaviors of DN-1.2 and DN-2.0-0.1, and between those of DN-N2 and DN-U1.

Table 3. A list of formulations and the existence of necking in the DN gels determined by uniaxial tensile tests, as shown in Fig. 6a.

Sample code	1st network			2nd network			Tensile behavior	G_{jump} [J/m^2]	G_{th} [J/m^2]
	AMPS [M]	MBAA [mol%]	α-keto [mol%]	AAm [M]	MBAA [mol%]	α-keto [mol%]			
DN-N1	1	2	1	2.0	0.01	0.01	Necking	–	$\approx 1.35 \times 10^3$
DN-N2	1	4	1	2.0	0.01	0.01	Necking	–	$\approx 2.0 \times 10^3$
DN-U1	1	4	0.1	2.0	0.1	0.1	Unnecking	$\approx 1.0 \times 10^3$	–

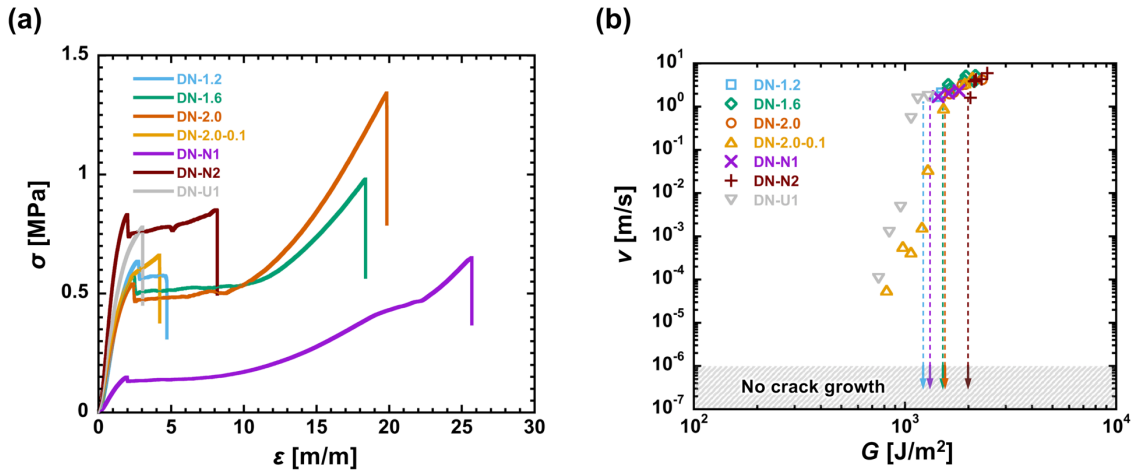

Fig. 6. (a) Uniaxial tensile stress–strain curves and (b) logarithmic plots of the energy release rate G and the velocity of crack growth v for all necking and unnecking DN gels with different network compositions. The sample codes are provided in Table 3. The arrows depict the G at which crack propagation was not detected. The grey hatched regime indicates the crack propagation was not observed within experimental resolution.

3.3 Real-Time Birefringence Observation During Crack Growth

To clarify the reason for the suppression of slow-mode crack propagation by necking DN gels, we examined the optical retardation images around the crack tips of DN gels to identify the necking zones in which the second networks were in highly anisotropic orientations. Previous studies have suggested that, for a necking DN gel, the brittle first network ruptures into clusters above the yielding point with necking [2], and the stretchable second network holds the stress with microscopic elongation along the tensile direction [7]. The degree of molecular orientation of the networks can be determined by retardation R.

Figures 7a–c show the optical retardation images for the representative samples. There was a large difference between the R distributions around the crack tips of brittle DN-0.8

with slow-mode crack propagation and the necking DN-2.0 without crack propagation, which suggested the contribution of microscopic molecular conditions to the suppression of slow-mode crack propagation. In the case of brittle DN-0.8, no high R area around the crack tip was observed during slow-mode crack propagation. This implied that the sparse second networks were not sufficiently strong to bear the load transferred from the broken first networks; therefore, the two networks broke together at slow speeds. In contrast, in the case of necking DN-2.0, a distinctly strong triangular R area was developed around the crack tip at G prior to crack propagation. The size of the strong R area was on the millimeter scale in both parallel and perpendicular directions to the stretch direction. The maximum R at the crack tip (R_{max} = 97.9 nm) was approximately 10 times the average R in the bulk (R_{bulk} = 10 nm). This suggested that the dense second network was strong enough to bear the load transferred from the fractured first networks around the crack tips. Moreover, the large strain hardening of the second network further induced fracture of the first network in the crack tip area, which suppressed crack propagation. The large damage zone generated before crack propagation is in agreement with our previous observations [5,30,40]. This high crack resistance induced by partial stretching of flexible networks from fractured rigid networks is specific to the DN structures consisting of contrasting networks. However, at G where the crack propagated in fast mode, R becomes very weak. For unnecking DN-2.0-0.1, a slightly high crescent moon-shaped R area was noticed at the crack tip (Fig. 7c), which was substantially smaller than the triangular R area of necking DN-2.0.

Next, we calculated the areas S having higher R than that of the bulk for different G values for necking DN-2.0. Here S was determined as area for R 2 times higher than that of bulk region. The calculated S might not be sufficiently accurate because of variations in manual notching or the resolution limitation of R images. Nevertheless, we observed a decreasing tendency in S with the increase of G near G_{th} (Fig. 7d). In addition, the R_{max} intensity around the crack tip also decreased once G exceeded G_{th}. These results indicate that the disappearance of the damage zone and the fast-mode crack propagation are intrinsically related. The energy required to form the damage zone sets a high energy barrier for the initiation of crack propagation. Once the energy release rate overcomes the energy barrier to form the damage zone, the crack starts to propagate. As the damage zone size reduces when the crack starts to propagate, the fracture energy decreases while energy release rate keeps constant. Therefore, the excess energy release accelerates the crack propagation, which results in fast mode fracture (brittle fracture).

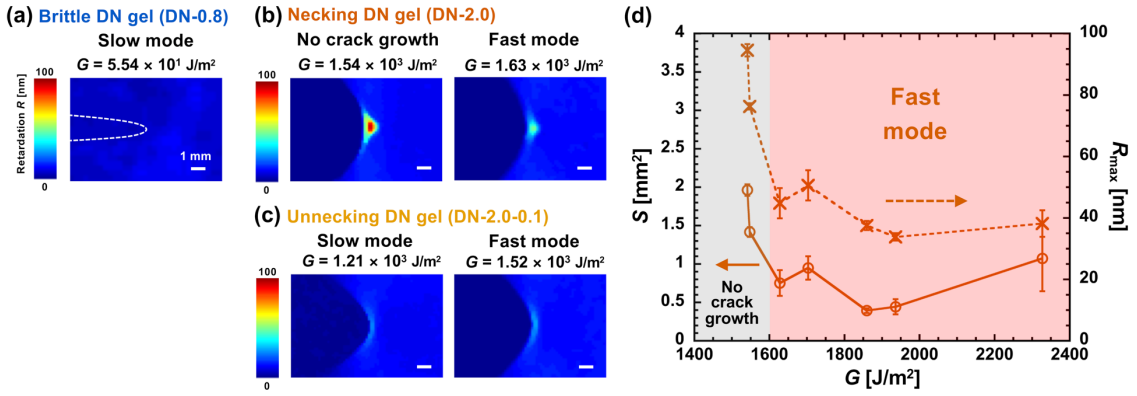

Fig. 7. Representative retardation images of (a) DN-0.8, (b) DN-2.0 and (c) DN-2.0-0.1. (d) Corresponding high retardation areas, S, and maximum retardations, R_{max}, at the crack tips of necking DN-2.0 as a function of the energy release rate G. Scale bars represent 1 mm. The white dashed curve in (a) depicts the crack shape of DN-0.8.

3.4 Discussion

3.4.1 Velocity transition

Sakumichi *et al.* and Kubo *et al*. explained the velocity jump of viscoelastic rubbers by a rubber–glass transition around the crack tip with an increase in the strain rate [41,42]. Here we discuss if this explanation is applicable to the slow-to-fast mode transition of hydrogels observed in Fig. 4a for SN and unnecking DN gels. According to the polymer network theory, the dynamics of chemically crosslinked gels is characterized by two relaxation times, the longest Rouse relaxation time τ_R of polymer strands between crosslinking points, and the relaxation time of Kuhn segment τ_0 [43]. Depending on the strain rate ω, crosslinked gels behave elastically at $\omega < \tau_R^{-1}$ with an ω-independent modulus (plateau modulus), viscoelastically at $\tau_R^{-1} < \omega < \tau_0^{-1}$ with a modulus increasing with $\omega^{1/2}$, and glassy like at $\omega > \tau_0^{-1}$ with a high modulus. τ_R depends on the network structure, while τ_0 only depends on Kuhn segment size and is ~10^{-9} s^1 for the synthetic flexible polymers [43]. To discuss the dynamic behavior of the polymer network at the crack tip, we estimate the crack tip strain rate ω_{tip} in the slow mode regime. By rough order estimation, $\omega_{tip} \sim v/r$ where r is the distance from the crack tip [44,45]. The minimum r should be the mesh size ξ for a polymer network, which could be estimated from the Young's modulus using relation $E \approx 3k_BT/\xi^3$, where k_B and T are the Boltzmann' constant and absolute temperature, respectively [43,46]. For SN-2.0, $\tau_R \sim 10^{-4}$ s^1, which is obtained from a PAAm hydrogel with a comparable modulus [47]. On the other hand, the strain rate experienced by the polymer network near the crack tip was $\omega_{tip} \sim 10^4$–10^5 s^{-1} for $v \sim 10^{-4}$–10^{-3} m/s using $\xi \sim 8.8$ nm ($E = 18.1$ kPa, Table 2). Accordingly, at the crack tip, $\omega_{tip}\tau_R \sim 1$–10, and the network responses viscoelastically. This explains the v-dependence of $\Gamma(v)$ even in the slow mode regime. However, since $\omega_{tip}\tau_0 \sim 10^{-4} << 1$ even for the maximum velocity before the velocity jump (~ 10^{-3} m/s), the slow-to-fast mode

transition could not be explained by the rubber-glass transition around the crack tip for the SN gel. We consider that when G increased to the G_{jump}, $G = \Gamma$ is no longer hold, and the excess energy release rate, $G - \Gamma > 0$, might accelerates the crack propagation to fast mode. Later, the accelerated crack is affected by inertia effect, which results in the steady-state v at fast mode [36]. Consequently, we observed a sudden velocity jump at G_{jump}. The same explanation could be applied to the velocity jump of brittle DN gel and unnecking DN gel, which show the maximum velocity before the velocity jump of ~ 10^{-3}–10^{-2} m/s.

3.4.2 Suppression of slow mode in necking DN gels

The results of crack growth tests and birefringence observations suggest that the existence of a large damage zone around the crack tip plays an important role in the suppression of slow-mode crack propagation. To understand why the slow-mode crack propagation is suppressed for the necking DN gels, we discussed the energy balances of the necking DN gels during crack initiation. As reported in previous studies [24,48], the fracture energy at crack initiation Γ_c can be described as follows:

$$\Gamma_c = \Gamma_0 + \Gamma_{dis} \approx \Gamma_0 + U_{dis}h \qquad (3)$$

where Γ_0 is the intrinsic Γ of the damage zone, Γ_{dis} is the dissipated energy because of the formation of the damage zone, U_{dis} is the mechanical hysteresis density, and h is the characteristic size of the damage zone defined in the undeformed state in the stretching direction. When G approaches Γ_c, damage zones with long h around the crack tips develop in the necking DN gels, which results in an extraordinarily high Γ_c.

Theoretical results indicate that near the crack tip, uniaxial tension dominates for a highly deformable soft solid under mode-I plane-stress conditions [49]. Using this uniaxial approximation, we can roughly consider that U_{dis} is equal to the work of extension to fracture W_f of the unnotched sample under uniaxial tension, namely, $U_{dis} \approx W_f$. If we suppose that $\Gamma_{dis} >> \Gamma_0$ at the onset of crack initiation ($G = G_{th} \approx \Gamma_c$), equation (4) can be presented as

$$G_{th} \approx W_f h \qquad (4),$$

which provides

$$h \approx G_{th} / W_f \qquad (5)$$

In the case of DN-2.0, h was estimated to be ≈ 132 μm from equation (5) using $W_f \approx 12.1$ MJ/m^3 and $G_{th} \approx 1.6 \times 10^3$ J/m^2 obtained by uniaxial tensile tests and crack growth tests. Because h is the undeformed size of the damage zone, h multiplied by the fracture stretch ratio λ_f (≈ 18.0) affords the damage zone in the deformed state, which was estimated as

$h\lambda_f \approx 2.4$ mm. This value is almost identical to the height of the high R area at $G \leq G_{th}$ acquired by the R images, that is, ~ 2.76 mm (Fig. 7b). This justifies again that the high Γ_c of the necking DN gels is due to their large damage zones, as described in equation (3). Subsequently, we discussed the energy balance after crack initiation. Once G reaches G_{th} and the crack starts to propagate, the damage zone cannot develop for the necking DN samples, as indicated by the reduction of S and R_{max} in Fig. 7d. Therefore, Γ_{dis} decreases, and Γ becomes less than that at crack initiation, namely, $\Gamma < \Gamma_c$. The excessive energy release $G - \Gamma > 0$ at onset of crack propagation leads to crack acceleration. This explains why the necking DN gels show only fast-mode crack propagation.

Then, the final question is why the damage zone disappears at $G > G_{th}$ after crack initiation? We consider that this phenomenon is also related to the dynamics of the polymer network. The damage zone develops via continuous internal deformation and load transfer process, including loading and breakage of the first network, transfer of load to the second network, deformation and strain hardening of the second network to induce further breakage of the first network. Such process should repeat until the tension on the surface of the crack becomes high enough to activate the breakage of second network strands on the surface, and the larger the damage zone, the longer the time required for this process. Therefore, for the necking DN gels, once the crack starts to propagate even at in slow speed, the strain rate at the crack tip is already high in viscoelastic regime ($\omega_{tip}\tau_R > 1$), therefore, there is insufficient time for the formation of a damage zone far from the crack tip. Our recent study on the crack initiation of pre-notched necking DN gels also suggests a strong influence of the second network dynamics on the size of damage zone [50].

4. Conclusions

Crack propagation of DN hydrogels under various tensions was systematically studied for the first time. Strong correlations between the crack growth behaviors of the DN gels under tension and their uniaxial tensile behaviors were observed. The crack growth velocity v of the brittle or unnecking DN gels exhibited slow mode at relatively low strain energy release rate G and it jumped to the fast mode above a critical G_{jump}, in similar to SN gels and rubbery materials reported. In contrast, for the necking DN gels, the crack propagation was initiated at a very high threshold G_{th}, above which the crack propagated at fast mode, without via the slow mode. We found that the large threshold G_{th} and the suppression of the slow-mode crack propagation in the necking DN gels were related to the creation of damage zone around the crack tip. A large damage zone was formed at G slightly smaller than G_{th}, prior to the crack propagation, while the damage zone almost vanished once the crack started to propagate above G_{th}. The damage zone formation, which consumes large amount of energy due to breaking of the brittle sacrificial network, sets a high energy barrier for crack initiation; once the crack starts to propagate, the crack propagation is too fast to allow the full development of damage zone. As a result, the

elastic energy released by the overstretched DN gels surpasses the fracture energy for crack advancing, and the crack is accelerated to reach the fast mode. Accordingly, we consider that the unique behavior of necking DN gels is attributed to insufficient time for damage zone formation at the crack tip. The large G_{th} demonstrates the excellent crack initiation resistance Γ_c (= G_{th}) of necking DN gels under high tension. We believe that the unique crack resistance characterized in this work is important for practical design of DN gels as load-bearing materials.

Acknowledgments

This research was funded by the Japan Society for the Promotion of Science JSPS KAKENHI (grant no. JP17H06144) and by the ImPACT Program of the Council for Science, Technology and Innovation (Cabinet Office, Government of Japan). Y. Z. thanks financial support from MEXT through the Program for Leading Graduate Schools (Hokkaido University "Ambitious Leader's Program").

References

[1] J. P. Gong, Y. Katsuyama, T. Kurokawa, Y. Osada, Double-Network Hydrogels with Extremely High Mechanical Strength, Adv. Mater. 15 (2003) 1155–1158. https://doi.org/10.1002/adma.200304907.

[2] J. P. Gong, Why Are Double Network Hydrogels so Tough?, Soft Matter 6 (2010) 2583–2590. https://doi.org/10.1039/b924290b.

[3] T. Nakajima, Generalization of the Sacrificial Bond Principle for Gel and Elastomer Toughening, Polym. J. 49 (2017) 477–485. https://doi.org/10.1038/pj.2017.12.

[4] Y. Tanaka, R. Kuwabara, Y. H. Na, T. Kurokawa, J. P. Gong, Y. Osada, Determination of Fracture Energy of High Strength Double Network Hydrogels, J. Phys. Chem. B 109 (2005) 11559–11562. https://doi.org/10.1021/jp0500790.

[5] Q. M. Yu, Y. Tanaka, H. Furukawa, T. Kurokawa, J. P. Gong, Direct Observation of Damage Zone around Crack Tips in Double-Network Gels, Macromolecules 42 (2009) 3852–3855. https://doi.org/10.1021/ma900622s.

[6] R. E. Webber, C. Creton, H. R. Brown, J. P. Gong, Large Strain Hysteresis and Mullins Effect of Tough Double-Network Hydrogels, Macromolecules 40 (2007) 2919–2927. https://doi.org/10.1021/ma062924y.

[7] T. Nakajima, T. Kurokawa, S. Ahmed, W. Wu, J. P. Gong, Characterization of Internal Fracture Process of Double Network Hydrogels under Uniaxial Elongation, Soft Matter 9 (2013) 1955–1966. https://doi.org/10.1039/C2SM27232F.

[8] E. Ducrot, Y. Chen, M. Bulters, R. P. Sijbesma, C. Creton, Toughening Elastomers with Sacrificial Bonds and Watching Them Break, Science 344 (2014) 186–189. https://doi.org/10.1126/science.1248494.

[9] T. T. Mai, T. Matsuda, T. Nakajima, J. P. Gong, K. Urayama, Distinctive Characteristics of Internal Fracture in Tough Double Network Hydrogels Revealed by Various Modes of Stretching, Macromolecules 51 (2018) 5245–5257. https://doi.org/10.1021/acs.macromol.8b01033.

[10] K. Fukao, T. Nakajima, T. Nonoyama, T. Kurokawa, T. Kawai, J. P. Gong, Effect of Relative Strength of Two Networks on the Internal Fracture Process of Double Network Hydrogels As Revealed by *in Situ* Small-Angle X-Ray Scattering, Macromolecules 53 (2020) 1154–1163. https://doi.org/10.1021/acs.macromol.9b02562.

[11] Y. Tanaka, Y. Kawauchi, T. Kurokawa, H. Furukawa, T. Okajima, J. P. Gong, Localized Yielding around Crack Tips of Double-Network Gels, Macromol. Rapid Commun. 29 (2008) 1514–1520. https://doi.org/10.1002/marc.200800227.

[12] Y. H. Na, Y. Tanaka, Y. Kawauchi, H. Furukawa, T. Sumiyoshi, J. P. Gong, Y. Osada, Necking Phenomenon of Double-Network Gels, Macromolecules 39 (2006) 4641–4645. https://doi.org/10.1021/ma060568d.

[13] T. Matsuda, T. Nakajima, Y. Fukuda, W. Hong, T. Sakai, T. Kurokawa, U. Il Chung, J. P. Gong, Yielding Criteria of Double Network Hydrogels, Macromolecules 49 (2016) 1865–1872. https://doi.org/10.1021/acs.macromol.5b02592.

[14] W. Yang, H. Furukawa, J. P. Gong, Highly Extensible Double-Network Gels with Self-Assembling Anisotropic Structure, Adv. Mater. 20 (2008) 4499–4503. https://doi.org/10.1002/adma.200801396.

[15] T. Nakajima, N. Takedomi, T. Kurokawa, H. Furukawa, J. P. Gong, A Facile Method for Synthesizing Free-Shaped and Tough Double Network Hydrogels Using Physically Crosslinked Poly(Vinyl Alcohol) as an Internal Mold, Polym. Chem. 1 (2010) 693–697. https://doi.org/10.1039/c0py00031k.

[16] T. Nakajima, H. Sato, Y. Zhao, S. Kawahara, T. Kurokawa, K. Sugahara, J. P. Gong, A Universal Molecular Stent Method to Toughen Any Hydrogels Based on Double Network Concept, Adv. Funct. Mater. 22 (2012) 4426–4432. https://doi.org/10.1002/adfm.201200809.

[17] J.-Y. Sun, X. Zhao, W. R. K. Illeperuma, O. Chaudhuri, K. H. Oh, D. J. Mooney, J. J. Vlassak, Z. Suo, Highly Stretchable and Tough Hydrogels, Nature 489 (2012) 133–136. https://doi.org/10.1038/nature11409.

[18] T. Matsuda, T. Nakajima, J. P. Gong, Fabrication of Tough and Stretchable Hybrid Double-Network Elastomers Using Ionic Dissociation of Polyelectrolyte in Nonaqueous Media, Chem. Mater. 31 (2019) 3766–3776. https://doi.org/10.1021/acs.chemmater.9b00871.

[19] Y. Zheng, R. Kiyama, T. Matsuda, K. Cui, X. Li, W. Cui, Y. Guo, T. Nakajima, T. Kurokawa, J. P. Gong, Nanophase Separation in Immiscible Double Network Elastomers Induces Synergetic Strengthening, Toughening, and Fatigue

Resistance, Chem. Mater. 33 (2021) 3321–3334. https://doi.org/10.1021/acs.chemmater.1c00512.
[20] X. Feng, Z. Ma, J. V. MacArthur, C. J. Giuffre, A. F. Bastawros, W. Hong, A Highly Stretchable Double-Network Composite, Soft Matter 12 (2016) 8999–9006. https://doi.org/10.1039/c6sm01781a.
[21] D. R. King, T. Okumura, R. Takahashi, T. Kurokawa, J. P. Gong, Macroscale Double Networks: Design Criteria for Optimizing Strength and Toughness, ACS Appl. Mater. Interfaces 11 (2019) 35343–35353. https://doi.org/10.1021/acsami.9b12935.
[22] T. Okumura, R. Takahashi, K. Hagita, D. R. King, J. P. Gong, Improving the Strength and Toughness of Macroscale Double Networks by Exploiting Poisson's Ratio Mismatch, Sci. Rep. 11 (2021) 1–13. https://doi.org/10.1038/s41598-021-92773-0.
[23] S. Ahmed, T. Nakajima, T. Kurokawa, M. Anamul Haque, J. P. Gong, Brittle-Ductile Transition of Double Network Hydrogels: Mechanical Balance of Two Networks as the Key Factor, Polymer 55 (2014) 914–923. https://doi.org/10.1016/j.polymer.2013.12.066.
[24] T. Nakajima, T. Kurokawa, H. Furukawa, J. P. Gong, Effect of the Constituent Networks of Double-Network Gels on Their Mechanical Properties and Energy Dissipation Process, Soft Matter 16 (2020) 8618–8627. https://doi.org/10.1039/d0sm01057j.
[25] W. Zhang, X. Liu, J. Wang, J. Tang, J. Hu, T. Lu, Z. Suo, Fatigue of Double-Network Hydrogels, Eng. Fract. Mech. 187 (2018) 74–93. https://doi.org/10.1016/j.engfracmech.2017.10.018.
[26] D. Kaneko, T. Tada, T. Kurokawa, J. P. Gong, Y. Osada, Mechanically Strong Hydrogels with Ultra-Low Frictional Coefficients, Adv. Mater. 17 (2005) 535–538. https://doi.org/10.1002/adma.200400739.
[27] K. Yasuda, N. Kitamura, J. P. Gong, K. Arakaki, H. J. Kwon, S. Onodera, Y. M. Chen, T. Kurokawa, F. Kanaya, Y. Ohmiya, Y. Osada, A Novel Double-Network Hydrogel Induces Spontaneous Articular Cartilage Regeneration *in Vivo* in a Large Osteochondral Defect, Macromol. Biosci. 9 (2009) 307–316. https://doi.org/10.1002/mabi.200800223.
[28] T. Nakajima, H. Furukawa, Y. Tanaka, T. Kurokawa, Y. Osada, J. P. Gong, True Chemical Structure of Double Network Hydrogels, Macromolecules 42 (2009) 2184–2189. https://doi.org/10.1021/ma802148p.
[29] S. Liang, J. Hu, Z. L. Wu, T. Kurokawa, J. P. Gong, Toughness Enhancement and Stick-Slip Tearing of Double-Network Hydrogels in Poly(Ethylene Glycol) Solution, Macromolecules 45 (2012) 4758–4763. https://doi.org/10.1021/ma300357f.
[30] T. Matsuda, R. Kawakami, T. Nakajima, J. P. Gong, Crack Tip Field of a

Double-Network Gel: Visualizing Covalent Bond Scission by Mechanoradical Polymerization, Macromolecules 53 (2020) 8787–8795. https://doi.org/10.26434/chemrxiv.12555419.
[31] Y. Morishita, K. Tsunoda, K. Urayama, Velocity Transition in the Crack Growth Dynamics of Filled Elastomers: Contributions of Nonlinear Viscoelasticity, Phys. Rev. E 93 (2016) 1–11. https://doi.org/10.1103/PhysRevE.93.043001.
[32] Y. Morishita, K. Tsunoda, K. Urayama, Crack-Tip Shape in the Crack-Growth Rate Transition of Filled Elastomers, Polymer 108 (2017) 230–241. https://doi.org/10.1016/j.polymer.2016.11.041.
[33] Y. Morishita, K. Tsunoda, K. Urayama, Universal Relation between Crack-Growth Dynamics and Viscoelasticity in Glass-Rubber Transition for Filled Elastomers, Polymer (Guildf). 179 (2019) 121651. https://doi.org/10.1016/j.polymer.2019.121651.
[34] I. Kolvin, J. M. Kolinski, J. P. Gong, J. Fineberg, How Supertough Gels Break, Phys. Rev. Lett. 121 (2018) 135501. https://doi.org/10.1103/PhysRevLett.121.135501.
[35] T. Onuma, Y. Otani, A Development of Two-Dimensional Birefringence Distribution Measurement System with a Sampling Rate of 1.3 MHz, Opt. Commun. 315 (2014) 69–73. https://doi.org/10.1016/j.optcom.2013.10.086.
[36] T. Goldman, A. Livne, J. Fineberg, Acquisition of Inertia by a Moving Crack, Phys. Rev. Lett. 104 (2010) 5–8. https://doi.org/10.1103/PhysRevLett.104.114301.
[37] R. S. Rivlin, A. G. Thomas, Rupture of Rubber. I. Characteristic Energy for Tearing, J. Polym. Sci. 10 (1953) 291–318. https://doi.org/10.1002/pol.1953.120100303.
[38] R. Long, C.-Y. Hui, Fracture Toughness of Hydrogels: Measurement and Interpretation, Soft Matter 12 (2016) 8069–8086. https://doi.org/10.1039/C6SM01694D.
[39] K. Tsunoda, J. J. C. Busfield, C. K. L. Davies, A. G. Thomas, Effect of Materials Variables on the Tear Behaviour of a Non-Crystallizing Elastomer, J. Mater. Sci. 35 (2000) 5187–5198. https://doi.org/10.1023/A:1004860522186.
[40] S. Liang, Z. L. Wu, J. Hu, T. Kurokawa, Q. M. Yu, J. P. Gong, Direct Observation on the Surface Fracture of Ultrathin Film Double-Network Hydrogels, Macromolecules 44 (2011) 3016–3020. https://doi.org/10.1021/ma2000527.
[41] N. Sakumichi, K. Okumura, Exactly Solvable Model for a Velocity Jump Observed in Crack Propagation in Viscoelastic Sheets, Sci. Rep. 7 (2016) 1–11. https://doi.org/10.1038/s41598-017-07214-8.
[42] A. Kubo, N. Sakumichi, Y. Morishita, K. Okumura, K. Tsunoda, K. Urayama, Y. Umeno, Dynamic Glass Transition Dramatically Accelerates Crack Propagation

in Rubberlike Solids, Phys. Rev. Mater. 5 (2021) 1–14. https://doi.org/10.1103/PhysRevMaterials.5.073608.
[43] M. Rubinstein, R. H. Colby, Polymer Physics; Oxford University Press, (2003).
[44] P. G. De Gennes, Soft Adhesives, Langmuir 12 (1996) 4497–4500. https://doi.org/10.1021/la950886y.
[45] B. N. J. Persson, O. Albohr, G. Heinrich, H. Ueba, Crack Propagation in Rubber-like Materials, J. Phys.: Condens. Matter 17 (2005) 1071-1142. https://doi.org/10.1088/0953-8984/17/44/R01.
[46] H. Guo, Y. Uehara, T. Matsuda, R. Kiyama, L. Li, J. Ahmed, Y. Katsuyama, T. Nonoyama, T. Kurokawa, Surface Charge Dominated Protein Absorption on Hydrogels, Soft Matter 16 (2020) 1897–1907. https://doi.org/10.1039/c9sm01999e.
[47] B. A. Krajina, C. Tropini, A. Zhu, P. Digiacomo, J. L. Sonnenburg, S. C. Heilshorn, A. J. Spakowitz, Dynamic Light Scattering Microrheology Reveals Multiscale Viscoelasticity of Polymer Gels and Precious Biological Materials, ACS Cent. Sci. 3 (2017) 1294–1303. https://doi.org/10.1021/acscentsci.7b00449.
[48] Y. Tanaka, A Local Damage Model for Anomalous High Toughness of Double-Network Gels, Europhys. Lett. 78 (2007) 56005. https://doi.org/10.1209/0295-5075/78/56005.
[49] R. Long, C. Y. Hui, Crack Tip Fields in Soft Elastic Solids Subjected to Large Quasi-Static Deformation - A Review, Extrem. Mech. Lett. 4 (2015) 131–155. https://doi.org/10.1016/j.eml.2015.06.002.
[50] Y. Zheng, T. Matsuda, T. Nakajima, W. Cui, Y. Zhang, C.-Y. Hui, T. Kurokawa, J. P. Gong, How Chain Dynamics Affects Crack Initiation in Double-Network Gels, Proc. Natl. Acad. Sci. 118 (2021) 1–8. https://doi.org/10.1073/pnas.2111880118.